World Applied Sciences Journal 17 (7): 882-890, 2012
ISSN 1818-4952

2-D Laminar Natural Convection Heat Transfer in Different Tilt Angles and Aspect Ratios Using Staggered and Collocated Approaches

Mohammad Saeedi and Shahin Nasseri Oskouie

Department of Mechanical and Manufacturing Engineering,
University of Manitoba, Winnipeg, Canada R3T 5V6

Abstract: 2-D laminar flow with natural Convection with different checker board removing approaches (staggered and collocated grid systems) is solved to provide comparison between staggered and collocated arrangements. SIMPLEC algorithm is employed for pressure velocity coupling. The results are first presented for a benchmark problem and then the effect of the inclination angle and aspect ratio are investigated. Mean Nusselt number, flow pattern and convergence characteristics are used for comparison. The convergence behaviour of two approaches is also tested for different Rayleigh numbers. Staggered arrangement generally had a better performance in that regard.

Key words: Staggered · Collocated · Convergence behaviour · Natural convection · Cavity

INTRODUCTION

Staggered and collocated approaches are both acceptable and common approaches for solving fluid flow problems. In terms of coding and application, each of them has some relative merits and advantages. However the most apparent difference between these two approaches is the capability of collocated grid arrangement in handling the complex geometries. Thus, comparison of these two approaches is an interesting subject in computational fluid dynamics. In 1988, Peric *et al*. [1] presented a detailed comparison of staggered and collocated grids on 2-D fluid flow problems. It was shown in their work that the convergence rate, dependency on under-relaxing parameters, computational effort and accuracy are almost identical for both grids however collocated grid had advantages when multi grid techniques or non-orthogonal grids are used. In 1999, Meier *et al*. [2] studied the performance of staggered and collocated grid arrangements for single and multi-phase flows in some different physical conditions. They showed that staggered arrangement had a better stability when high pressure gradient is present in the flow field. In the same year, Li *et al*. [3] investigated the performance of different convective schemes on 3-D heat and fluid flow problems with different grid systems. It was shown that all the tested schemes had the same behaviour on staggered and collocated grids. Natural convection phenomenon as an important application of fluid flow engineering can also be an interesting topic for comparing two mentioned approaches, however, not much work has been done in this view. This is why many researchers have studied natural convection but for the sake of physical studies and not for comparison of staggered and collocated approaches. In 1977, Raithby *et al*. [4] conducted an analytical investigation on natural convective heat transfer through different layers of fluid in a cavity with isothermal vertical walls and adiabatic horizontal walls. This analysis showed a good agreement with the experimental data. In 1978, Catton [5] presented a thorough review of the existing empirical relations to predict the natural convection heat transfer in rectangular cavities in different conditions. In 1983, Davis [6] numerically solved the 2D natural convection flow with differentially heated sidewalls. His results are widely used by other researchers as a benchmark solution to validate their numerical solutions. In 1985, Briggs *et al*. [7] experimentally studied a square cavity by means of Laser-Doppler Velocimeter and detected the existence of periodic laminar flow regimes at Rayleigh number above 3.0×10^6. In 1990, Hortmann *et al*. [8] applied the multi-grid method to solve the natural convection problem in a cavity to obtain an efficient numerical tool for laminar

Corresponding Author: Shahin Nasseri Oskouie, Department of Mechanical and Manufacturing Engineering, University of Manitoba, Winnipeg, Canada R3T 5V6.

Table 1: Fluid properties and cavity dimensions used in the calculations

Ra	ρ	μ	β	Pr	g	T_h	T_c	L	H
10^3	0.37631	1.8×10^{-5}	0.00341	0.71	9.81	12	2	0.021277	0.021277
10^4	1.19	1.8×10^{-5}	0.00341	0.71	9.81	12	2	0.021277	0.021277
10^5	3.7631	1.8×10^{-5}	0.00341	0.71	9.81	12	2	0.021277	0.021277
10^6	11.9	1.8×10^{-5}	0.00341	0.71	9.81	12	2	0.021277	0.021277

buoyancy driven flows. In 1994, Lightstone *et al*. [9] solved the natural convection problem numerically as an assessment of their method to extend it to solve the hydrogen dispersion and heat transfer in nuclear power plants. In 2001, Frederick *et al*. [10] solved the 3D natural convection problem in a cube with a cold vertical wall and a hot square sector on the opposite wall over a set of temperature ranges to investigate the flow field and the transition Rayleigh number. In 2007, Bairi *et al*. [11] conducted a numerical and experimental study of natural convection in cavities with different tilt angles and with aspect ratios of 0.75 and 1.5. This work also presented a Nusselt-Rayleigh correlation suitable for convection heat transfer estimation. Aydin *et al*. [12], numerically studied the 2D natural convection flow in a square with localized heating from the bottom wall and symmetrical cooling from sides to investigate the effect of non-dimensional heat source length. Mariani *et al*. [13], investigated the effect of heat source on the bottom wall of a 2D rectangular cavity with different aspect ratios to determine the effect of heat source locations for controlling the flow. D'Orazio *et al*. [14], studied a rectangular cavity heated from the bottom wall and cooled from the top wall to investigate the effect of aspect ratio on this type of flow, the flow pattern was tracked at different Rayleigh numbers and aspect ratios and they found the Nusselt number variation pattern at the mentioned conditions. In 2007, Dong *et al*. [15] applied the lattice Boltzmann method to predict the natural convection flow in an enclosure and investigated the effect of the aspect ratio on the heat transfer.

In the present work, the results and performance of two checker board removing approaches (staggered and collocated grid systems) in a 2-D natural convection problem will be compared. The Nusselt number, flow patterns and computational performance are studied at different Rayleigh numbers, tilt angles and aspect ratios for both grid arrangements.

Problem Description: The problem being considered is that of the 2-D flow inside a cavity with boundary conditions and geometrical configurations shown in Fig. 1. As it can be seen, at zero inclination angle, the horizontal walls are insulated and the vertical sides are at temperature T_h and T_c.

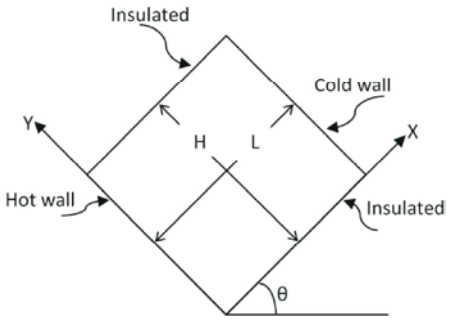

Fig. 1: Boundary conditions and geometrical configurations of the cavity

The solution of this problem has been obtained at Rayleigh number of 10^3, 10^4, 10^5 and 10^6. Table 1 shows the fluid properties and cavity dimensions used in the calculations.

Governing Equations and Solution Method: To solve the steady state natural convection in a square cavity for a Newtonian incompressible fluid, the continuity equation coupled with the incompressible version of the well-known Navier-Stokes equations containing the buoyancy force as a source term and also passive scalar transport equation for temperature have to be solved together. These equations are presented below.

$$\frac{\partial v_i}{\partial x_i} = 0 \tag{1}$$

$$\frac{\partial v_i}{\partial t} + v_j \frac{\partial v_i}{\partial x_j} = -\frac{\partial p}{\partial x_i} + \frac{\partial^2 v_i}{\partial x_j \partial x_j} + g_i \rho_{ref} \beta (T - T_{ref}) \tag{2}$$

$$\frac{\partial T}{\partial t} + v_j \frac{\partial T}{\partial x_j} = \alpha \frac{\partial^2 T}{\partial x_j \partial x_j} \tag{3}$$

The term $g_i\ \rho_{ref}\beta(T–T_{ref})$, the buoyancy force, comes from Boussinesq assumption in which β is the thermal expansion coefficient, g_i is the component of gravity force in i direction, ρ_{ref} and T_{ref} are reference density and temperature, respectively. Since the flow is incompressible, density is constant everywhere. The reference temperature is taken as the average temperatures of the hot and cold walls.

The transport equations are integrated over a finite number of control volumes, leading to a set of algebraic equations. The Central Differencing Scheme (CDS) is employed to discretize the diffusion terms, whereas a blending of upwind and central differencing is used for convection terms. The pressure–velocity coupling is achieved using the SIMPLEC method of Van Doormaal and Raithby [16]. The systems of algebraic equations are solved iteratively through a line by line application of the Thomas algorithm. The computational spatial domain is covered with an equidistance grid (160×160 CVs). The stopping criterion for the time loop is defined such that, the maximum difference of the solution variable between two successive iterations normalized by the range of the same variable should be less than 10^{-5}. When this criterion is met for all flow variables, the solution is considered to be steady state solution. It should be mentioned that all of the results presented in this study are grid independent.

Calculation of Mean Nusselt Number: In order to calculate the Nusselt number, the amount of heat transfer through the non-adiabatic walls need to be first calculated. Since the flow is steady, the absolute value of heat transfer from sidewalls must be identical. Equation (4) shows how to calculate the absolute value of heat transfer from walls, according to the Fourier heat conduction law, which is equal to the total convective heat transfer through the cavity.

$$Q = \frac{1}{thickness}\int kAdT_{absolute} = hA\Delta T_{(side\ walls)} \tag{4}$$

In which k is thermal conductivity, h is the convective heat transfer coefficient, A is the side wall area and T is temperature. Having found h from the above equation, mean Nusselt number can be found using equation (5).

$$\overline{Nu} = \frac{hL}{k} \tag{5}$$

In which L is the distance between hot and cold walls.

Benchmark Problem: In the first part, a benchmark test is done which is natural convection for air (Pr=0.71) in a square cavity with zero inclination angle heated and cooled from side walls at different Rayleigh numbers. The presented results are from independent grid which is 160×160 uniform grid. The results were then compared with those presented in Ref [6] and Ref [8]. Mean Nusselt number and streamline pattern contours will also be presented here.

Table 2: Comparison of mean Nusselt number for square cavity

Ra number	10^3	10^4	10^5	10^6
Ref. [8]	---	2.245	4.527	8.863
Ref. [6]	1.116	2.234	4.510	8.798
Present, staggered	1.119	2.246	4.547	8.863
Present, collocated	1.118	2.245	4.527	8.862

Table 2 presents the mean Nusselt number as a function of Rayleigh number obtained from staggered and collocated grids compared to Ref. [6] and Ref. [8] as a benchmark solution. Evidently, the agreement between the present work and Ref [6] and [8] is excellent and the maximum difference for staggered collocated gird is less than 0.7%. The Nusselt number is observed to have a direct relation with the Rayleigh number; a high Ra number leads to high Nu number. This trend is reasonable because the Rayleigh number (equation 6), is the product of Prandtl number (equation 7) and Grashof number (equation 8), which is responsible for buoyancy force. Increasing the Rayleigh number results in an increased Grashof number and thus increased buoyancy force. When the buoyancy force is increased, it causes a stronger convection field. This in turn will lead to a higher Nusselt number.

$$Ra = pr.\ Gr \tag{6}$$

$$pr = \mu c/k \tag{7}$$

$$Gr = \frac{g\beta\Delta TL^3}{\nu^3} \tag{8}$$

In which g, β, L and k have the same meaning as defined in previous equations. μ is the dynamic viscosity, c is the specific heat capacity of the medium, ΔT is the temperature difference between side walls, L is the distance between side walls and ν is the kinematic viscosity.

Figure 2 shows non-dimensional x and y velocity components along the vertical and horizontal lines respectively obtained from two grid arrangements. The velocity components are non-dimensionalized by diffusion velocity which is defined in equation (9).

$$V_{diff} = \mu/Pr\rho L \tag{9}$$

In this equation, μ is dynamic viscosity, Pr is the Prandtl number, ρ is density and L is the distance between hot and cold walls.

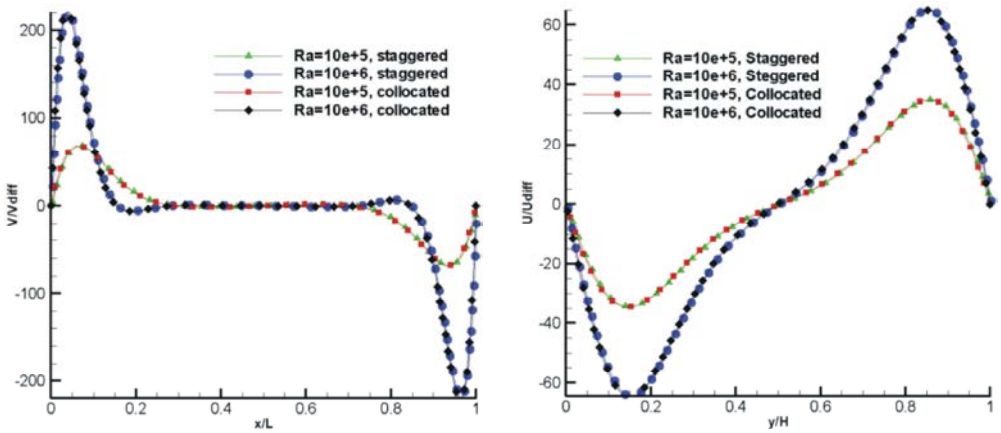

V/Vdiff U/Udiff

Fig. 2: Non-dimensional velocity components along horizontal and vertical mid lines

The results from two grid arrangements match very well and the curves are collapsed to each other. As evident in Figure 2, both U and V components are zero at walls due to no-slip condition. Furthermore, both velocity components are zero at the center of the cavity, which is because of the nearly stagnant condition in the center of the vortex formed in the centre of the cavity. The U and V distribution are also symmetric relative to the centre of the cavity as observed in Figure 2. Since the left wall is heated and the right one is cooled, the fluid is moving upward near the left wall (Positive V at $x/L \approx 0$) and is moving downward near the right wall (negative V at $x/L \approx 1$). These directions force the U component to be positive near the upper wall and to be negative near the lower wall and these all together mean the clock wise rotation of the fluid inside the cavity. Another noticeable point is that the maximum value of the non-dimensional V is greater than that of the non-dimensional U value. The reason is because the vertical walls are only heated and cooled and the effect of buoyancy is directly transferred to the fluid adjacent to the vertical walls.

As the Rayleigh number is increased the maximum values of the U and V components are observed to increase as well. This relation is a consequence of the higher buoyancy force generated at higher Rayleigh numbers. At $Ra=10^6$, it can be seen that after the largest peaks of the non-dimensional V curve which occur near the walls and moving toward the centre point, there is one oscillation observable with lower amplitude (compared to the main peaks). This secondary peak is due to secondary vertices (Figure 3d) formed between the cavity centre and the walls, however this effect is not observed in the U curve. The stream lines at different Rayleigh numbers are shown in Figures 3a-d. The clockwise motion of the fluid in the cavity may be observed. The secondary vertices that cause oscillation of the V contours for $Ra=10^6$ may be observed in Figure 3d. The mentioned vertices have no intersection with the central vertical line and this explains why there are no secondary peaks on the U curve. The symmetry relative to the cavity centre is also observable in all streamline patterns.

The stream lines at different Rayleigh numbers are shown in Figures 3a-d. The clockwise motion of the fluid in the cavity may be observed. The secondary vertices that cause oscillation of the V contours for $Ra=10^6$ may be observed in Figure 3d. The mentioned vertices have no intersection with the central vertical line and this explains why there are no secondary peaks on the U curve. The symmetry relative to the cavity centre is also observable in all streamline patterns.

The results presented in this section are in good agreement with those of Ref. [6] and can be considered as a validation for the present work. In the next section, the effect of tilt angle on the flow pattern and heat transfer will be investigated.

Tilted Square Cavities: In this section the effect of the inclination (tilt) angle on the Nusselt number and flow patterns will be examined. The inclination angle is defined as the angle between the insulated bottom wall (local X axis) and the horizontal line (Fig. 1). To simulate the flow in a tilted cavity, the components of gravitational acceleration in both x and y directions should be considered and then the gravity component should be applied to the relevant momentum equation.

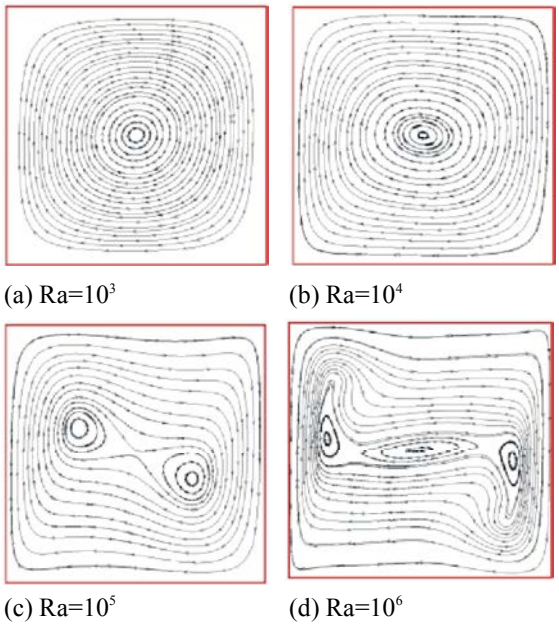

(a) Ra=10^3 (b) Ra=10^4

(c) Ra=10^5 (d) Ra=10^6

Fig. 3: Streamlines for different Rayleigh numbers

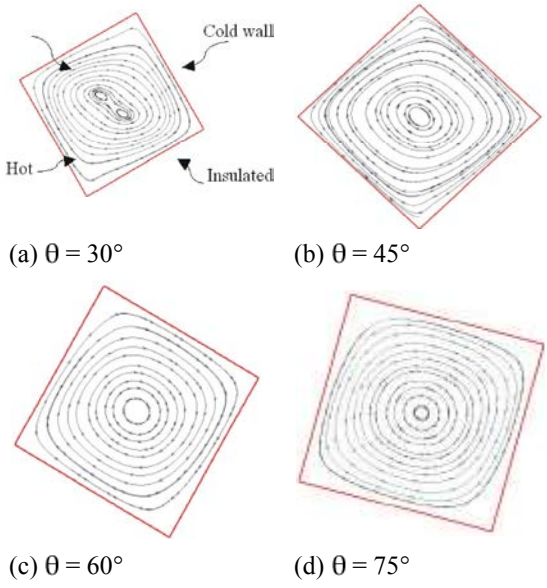

(a) θ = 30° (b) θ = 45°

(c) θ = 60° (d) θ = 75°

Fig. 4: Streamlines for different inclination angle and Ra=10^5

Figures 4a-d show the streamline patterns for different inclination angles and at Ra=10^5. These figures show that the greater the inclination angle is, the more deviation from horizontal pattern the streamlines will have. After θ = 45° the secondary vertices are not visible anymore and become merged into one single vortex which is more circular.

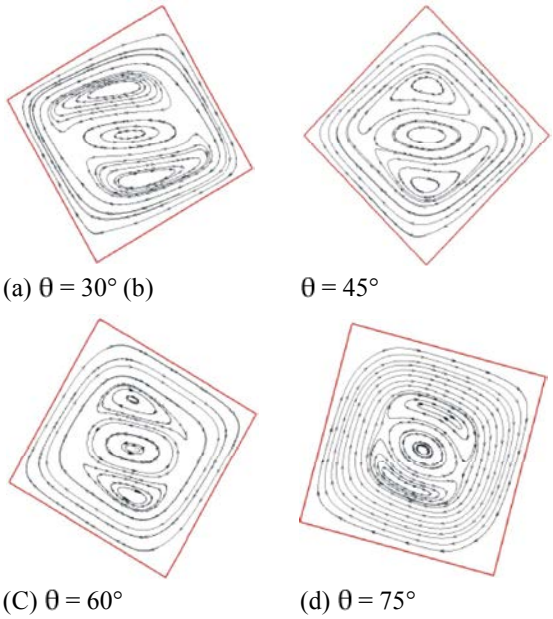

(a) θ = 30° (b) θ = 45°

(C) θ = 60° (d) θ = 75°

Fig. 5: Streamlines for different inclination angles and Ra=10^6

The streamline for different tilt angles at Ra=10^6 are also shown in Figure 5a-d. For this case, the secondary vertices do not disappear at any tilt angle but rather decrease as the inclination angle is increased. This behaviour is due to the strong buoyancy force at Ra=10^6. The vertical component is also strong enough to generate secondary vertices. The effect of the secondary vertices can be seen in the non-dimensional U and V distribution along horizontal and vertical lines in Figure 6.

Figures 6 shows the U and V distribution along lines parallel to the heated and insulated walls, passing through the centre of the cavity. Since the gravity is affecting the flow in the x and y directions (local x and y along insulated and heated walls respectively), the effect of secondary vertices for Ra=10^6 is observable for both the U and V distribution. The curves for all conditions are symmetric with respect to the cavity centre. The same symmetric behaviour is observable in the streamline patterns. As evident, the results obtained from staggered and collocated approaches under similar condition agree very well with each other and no major difference is visible.

Figures 7a-d show the temperature contours for different tilt angles at Ra=10^6. At θ = 45°, where gravity acts equally in both the x and y directions, the constant temperature lines in the middle of the cavity are almost

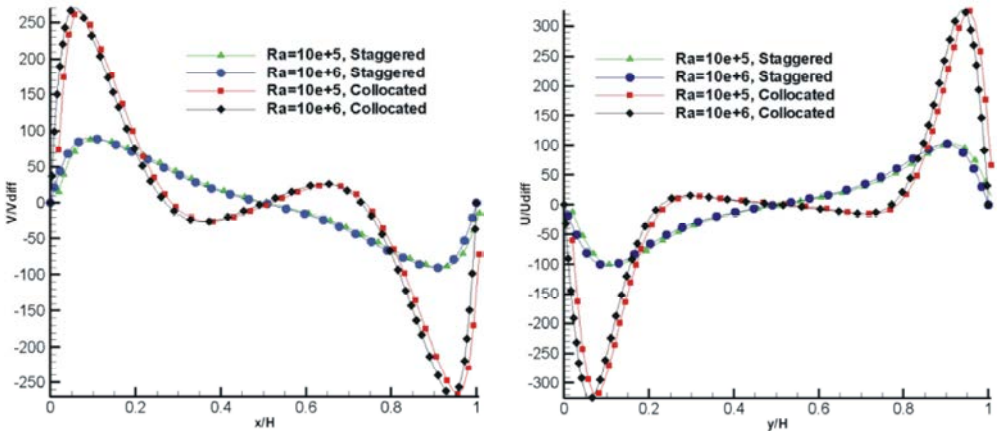

V/Vdiff U/Udiff

Fig. 6: Non-dimensional velocity components along local horizontal and vertical mid lines for $\theta = 60°$

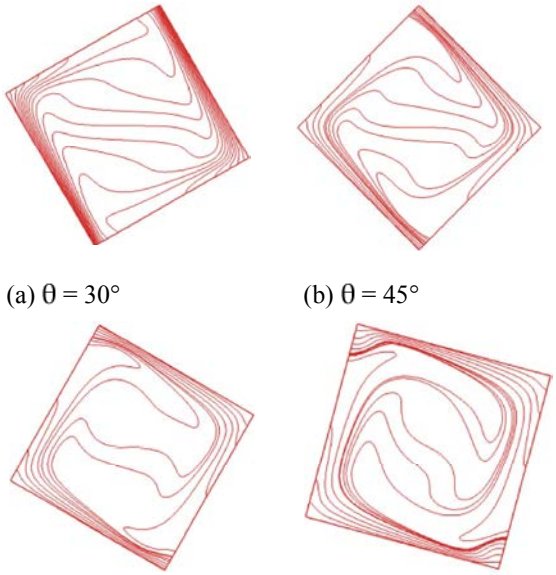

(a) $\theta = 30°$ (b) $\theta = 45°$

(c) $\theta = 60°$ (d) $\theta = 75°$

Fig. 7: Temperature contours for different inclination angle and $Ra=10^6$

along the horizontal, which shows the equal effect of U and V components on the temperature distribution. When the inclination angle is increased to 75°, the cavity is more like a cavity heated from below, rather than from sides. The pattern of the temperature contours is different from that of cavities with lower inclination angles as a result. Figures 8a-d show the variation of Nusselt number with inclination angle for different Rayleigh numbers. The maximum average Nusselt number is obtained when the inclination angle is between 30° to 40°. This fact can be explained considering that at $\theta = 30°$, temperature contours are denser near the hot and cold walls (Figure 7-a) which produce higher temperature gradient in these regions. When the inclination angle is increased more than the angle associated with the maximum Nusselt number, the gravity component along the hot wall is decreased and this causes the decrease of the Nusselt number.

Aspect Ratio: In this section the effect of the aspect ratio on the Nusselt number and flow patterns will be examined. Figures 9a-d show the stream line patterns for $Ra=10^5$. As it can be seen, by increasing the aspect ratio, the stream lines are stretched along vertical direction and the numbers of vortices also increase. The same trend is happened for $Ra=10^6$ in Figure 10a-d.

Figure 11 shows the effect of aspect ratio on Nusselt number for both grid systems compared with empirical formulas of [5]. As evident, by increasing the aspect ratio, the Nusselt number decreases and extrapolation can reveal that for very high aspect ratio the Nusselt number decreases to unity which means that the dominant heat transfer process is conduction. Again the good agreement between staggered and collocated approaches is clearly visible.

Convergence Behaviour: Table 3 shows the number of required loops to achieve the convergence criterion at different Rayleigh numbers for two grid systems. As shown in Table 3, in both grid systems, for higher

Table 3: Number of required time step to achieve the convergence criterion

Δt [s]		10^{-1}	10^{-2}	10^{-3}	10^{-4}	5×10^{-5}	10^{-5}	10^{-6}
$Ra=10^3$	Staggered	795	231	546	-----	-----	-----	-----
	Collocated	866	251	103165	-----	-----	-----	-----
$Ra=10^4$	Staggered	Not converged	257	407	-----	-----	-----	-----
	Collocated	1287	4374	-----	-----	-----	-----	-----
$Ra=10^5$	Staggered	Not converged	Not converged	291	2055	----	----	----
	Collocated	Not converged	Not converged	Not converged	Not converged	1731	6089	-----
$Ra=10^6$	Staggered	Not converged	Not converged	225	1350	-----	-----	-----
	Collocated	Not converged	Not converged	Not converged	Not converged	1291	4234	17914

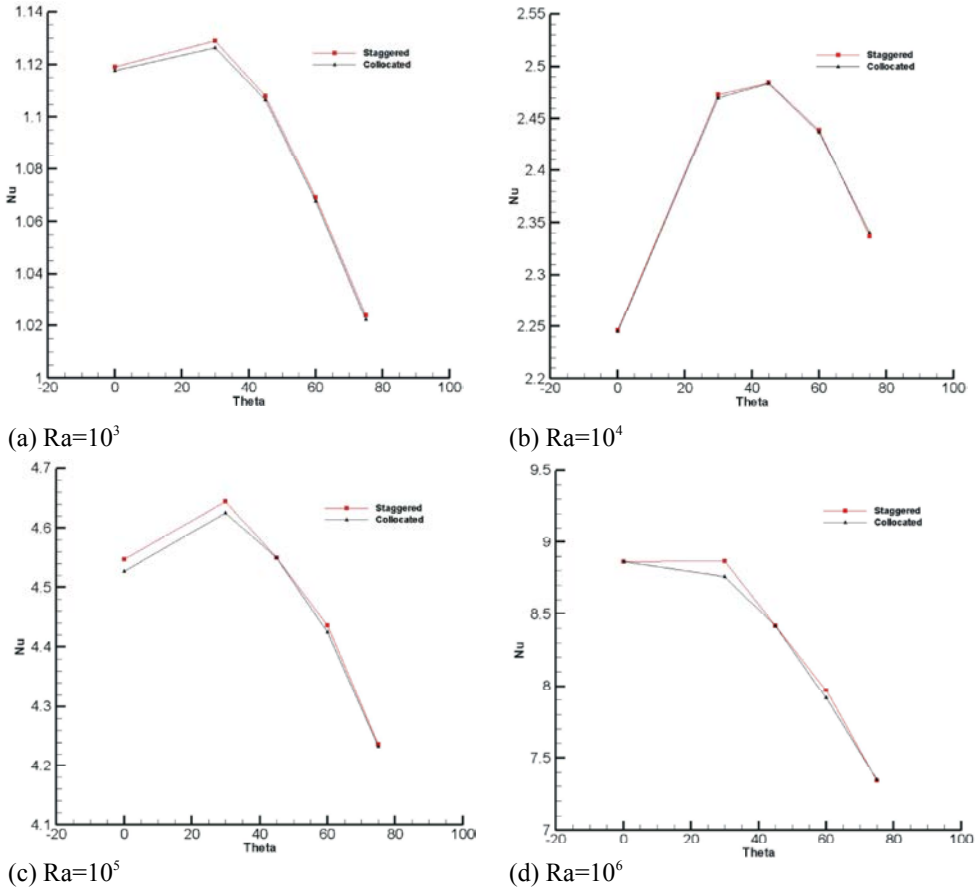

(a) $Ra=10^3$ (b) $Ra=10^4$

(c) $Ra=10^5$ (d) $Ra=10^6$

Fig. 8: Nusselt number variation with inclination angle for different Rayleigh numbers

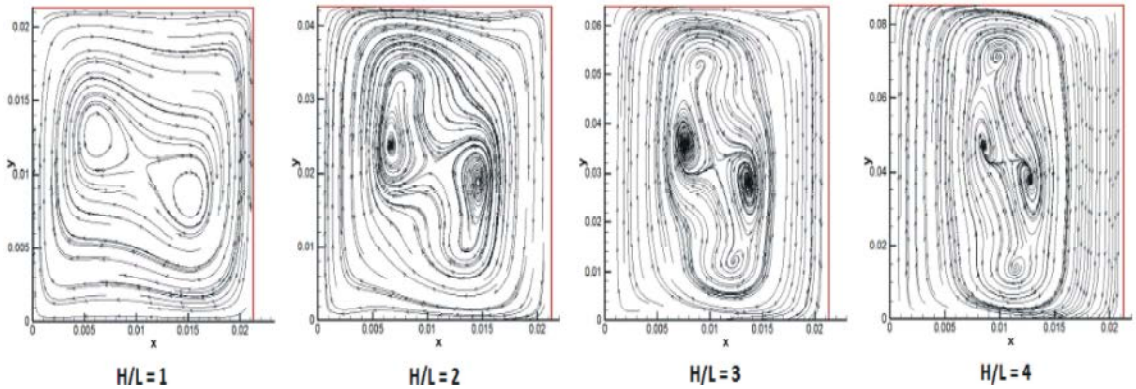

Fig. 9: Streamlines for different aspect ratios and $Ra=10^5$

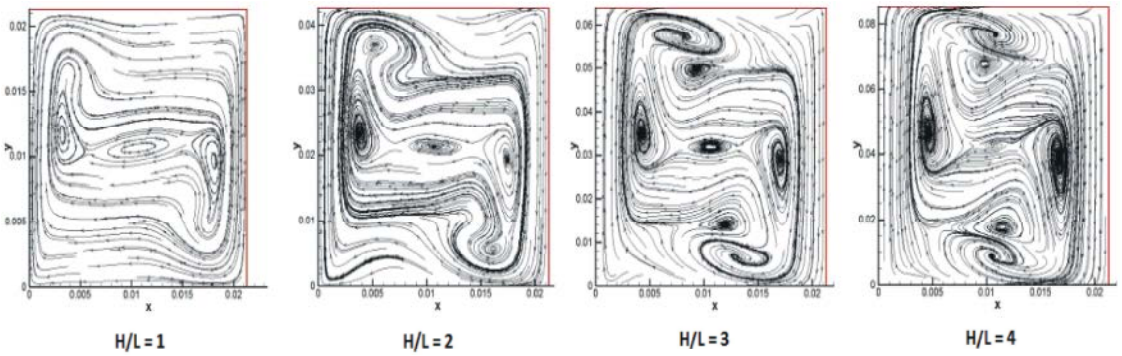

Fig. 10: Streamlines for different aspect ratios and Ra=10^6

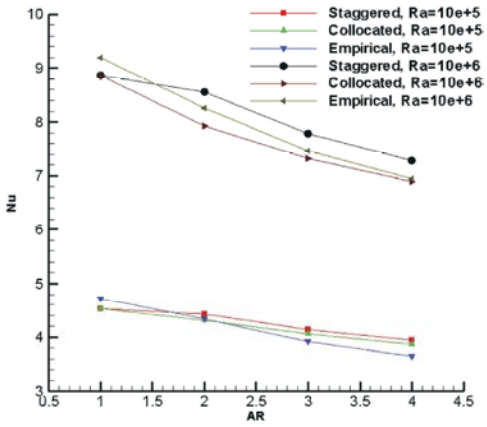

Fig. 11: Nusselt number variation with aspect ratios for different Rayleigh numbers

Rayleigh numbers, a finer time step is needed for convergence. This trend is due to higher buoyancy induced velocity at higher Rayleigh numbers. Table 3 also reveals that optimal time step for staggered approach is generally larger than that of collocated approach and this is more obvious when Rayleigh number is increased. Also, number of iterations at optimal time step is smaller for staggered approach.

CONCLUSION

2D laminar flow in a square cavity with natural convection is solved with two grid systems and the results at different Rayleigh numbers and different conditions were investigated. At the zero tilt angle, the flow characteristics were observed to be strongly dependent on the Rayleigh number. Increasing the Rayleigh number has been found to increase the Nusselt number. This phenomenon was an expected result, which matched the benchmark solution. When the cavity is rotated, variations of vortex formation and flow characteristics were observed in streamline patterns. At Ra=10^5, the secondary vertices disappeared when the inclination angle was increased, however, at Ra=10^6 the secondary vertices survived due to the stronger buoyancy force. When the inclination angle is between 30° to 40°, the average Nusselt number reaches its maximum value. Also, increasing the aspect ratio leads to decreased Nusselt number and extrapolation can reveal that for very high aspect ratio the Nusselt number decreases to unity which means that the dominant heat transfer process is conduction. A very good agreement between staggered and collocated grid systems was observed for all physical situations. In terms of convergence behaviour, staggered approach generally shows better behaviour which means larger time step and lower number of iterations required to converge to steady state solution.

REFERENCES

1. Peric, M., R. Kessler and G. Scheuerer, 1988. Comparison of Finite-Volume Numerical Methods with Staggered and Collocated Grids. Computers and Fluids, 16(4): 389-403.
2. Meier, H.F., J.J.N. Alves and M. Mori, 1999. Comparison between Staggered and Collocated grids in the Finite-Volume Method Performance for Sinlge and Multi-Phase Flows. Computer and Chemical Engineering, 23: 247-262.
3. Li, B., J. He and W. Tao, 1999. Six convective difference schemes on different grid systems for fluid flow and heat transfer with SIMPLE algorithm. J. Thermal Sci., 8(4): 250-261.
4. Raithby, G.D., K.G.T. Hollands and T.E. Unny, 1977. Analysis of Heat Transfer by Natural Convection Across Vertical Fluid Layers. J. Heat Transfer, 89: 287-293.

5. Catton, I., 1978. Natural Convection in Enclosures. Proceeding of 6th International Heat Transfer Conference, Toronto, Canada.
6. De Vahl Davis, G., 1983. Natural Convection of Air in a square Cavity: A Bench Mark Numerical Solution. International J. Numerical Methods in Fluids, 3: 149-164.
7. Briggs, D.G. and D.N. Jones, 1985. Two-dimensional Periodic Natural Convection in a Rectangular Enclosure of Aspect Ratio One. J. Heat Transfer, 107: 850-854.
8. Hortmann, M. and M. Peric, 1990. Finite Volume Multigrid Prediction of Laminar Natural Convection: Bench-Mark Solutions. International J. Numerical Methods in Fluids, 11: 189-207.
9. Lightstone, M.F. and W.M. Collins, 1994. Simulation of Natural Convection of Air in a Square Cavity Using the Gothic Thermal-Hydraulic Code. Proceeding of the CNA/CNS Annual Conference, Montreal, Canada.
10. Frederick, R.L. and F. Quiroz, 2001. On the Transition from Conduction to Convection Regime in a Cubical Enclosure with a Partially Heated Wall. International J. Heat and Mass Transfer, 44: 1699-1709.
11. Bairi, A., N. Laraqi and J.M. Garcia De Maria, 2007. Numerical and experimental study of natural convection in tilted parallelepipedic cavities for large Rayleigh numbers. Experimental Thermal and Fluid Sci., 31: 309-324.
12. Aydin, O. and W.J. Yang, 2000. Natural Convection in Enclosures with Localized Heating from below and Symmetrical Cooling from Sides. International J. Numerical Method for Heat and Fluid Flow, 10(5): 518-529.
13. Mariani, V.C. and L.S. Coleho, 2007. Natural Convection Heat Transfer in Partially open Enclosures Containing an Internal Local Heat Source. Brazilian J. Chemical Engineering, 24(3): 375-388.
14. D'Orazio, M.C., C. Cianfrini and M. Corcione, 2004. Rayleigh-Bénard convection in tall rectangular enclosures. International J. Thermal Sci., 43: 135-144.
15. Dong, Y. and Q. Zhai, 2007. Natural Convection in an Enclosure with Different Aspect Ratios. International J. Modern Physics, 18(12): 1903-1923.
16. Van Doormaal, J.P. and G.D. Raithby, 1984. Enhancement of the simple method for predicting incompressible fluid flows. Numerical Heat Transfer, 17: 147-163.